OPTICAL SYSTEM FOR ESS TARGET PROTECTION

M. Donna, T. Grandsaert, M. Göhran, R. Linander,
Thomas Shea, Cyrille Thomas*, ESS, Lund, Sweden

Abstract

One specificity of the ESS accelerator and target is that a high power and ultra low emittance proton beam is sent straight onto a Tungsten target. The high power density proton beam from the ESS linac will damage any material it meets. Thus a strategy to protect the target and the target area has to be deployed: the proton beam on target will be defocused and swept, distributing homogeneously the power density on an area 10^4 times larger than its non defocused area. On its way towards the target, the beam goes through two windows: the proton beam window (PBW) separating the high vacuum of the accelerator to the 1-bar He filled area of the target monolith; and the target window (TW) marking the entrance area of the target wheel. In this paper, we present the PBW imaging system, one of the proton beam diagnostics to be developed for imaging the proton beam current density deposited in the PBW. We will describe the expected performance of the imaging system in order to satisfy the PBW protection requirement. We will also describe the radiative processes which could be used as the source of the imaging system. Finally, we will describe the necessary condition and hardware for the implementation of a protection system for both the PBW and TW.

INTRODUCTION

The ESS Linac is designed to deliver a proton beam on a tungsten target for the production of neutrons. The emittance of the beam is 0.7 mm.mrad and its average power is 5 MW [1]. As a result, the natural beam size at the end of the linac, thus on target, is expected to be 2-3 mm, and would damage the target instantaneously. The strategy chosen to prevent this is twofold: the beam is defocused and swept linearly across a large area on the target [2]. The results is a dilution of the proton current density on the PBW and target by a factor 10^4, bringing the density bellow the damaging threshold (0.110 mA/cm^2 on PBW). However, each proton beam macro-pulse, a train of one million proton bunches, 2.86 ms long with more than 10^{15} protons in total, can potentially damage the PBW and TW if the defocusing and rastering condition are not fulfilled. In order to monitor the proton beam current density distribution of each macro-pulse, we will implement redundant diagnostics [2]. One of these will be to perform an image of the beam passing through the PBW. Each image will show the current density distribution which can be recorded, analysed in such a way that not only the degradation state of the PBW can be monitored and anticipated, but also any fault of the rastering system can be detected and beam abort before the next macro-pulse. In the following, we will present the imaging system performance required for PBW protection, together with the constraints from the high radiation environment of the target. We will also mention the possible sources to be used, emerging from the interaction of the protons with the surface of the PBW. Finally, we will draw the necessary condition for the PBW protection to occur, and present the possible hardware and software to implement such a protection system.

* cyrille.thomas@esss.se

IMAGING SYSTEM EXPECTED PERFORMANCE

The imaging system for the PBW has to meet performance for protection of the PBW, but also, to overcome the constraints due to the hard radiation environment. The PBW is large, with $250 \times 110\,\mathrm{mm}^2$. The first optical element of the imaging system can be placed at 2.65 m from the PBW, 65 mm above or bellow the proton beam axis. The optical system has to go through a 4 m high plug, the Proton Beam Instrumentation Plug (PBIP), in order to exit the high radiation area of the target; then the optical path has to run another 7 m toward a radiation safe environment for camera and people. In total the distance from the PBW to the image sensor is close to 15 m. The size of the sensor imposes magnification less than $m = 0.2$. The resolution is specified to be of the order of 1 mm or less. The transmission must be optimised not only to permit single shot macro-pulse imaging, but also reliable analysis on the images. The distortion of the image must also be minimised to render image fidelity and avoid additional image processing prior analysis of the current density distribution. Finally, because the first optical elements are in radiation environment, the optical path goes through the radiation shield and thus its integrity must remain. In addition, the first optical elements must be remote handled during installation and removal after been degraded by long exposure to the hadronic shower. The expected performances described above translate into optical characteristics, which in turn, can be summarised with a reduced number of these characteristics. The position of the PBIB and the necessary small aperture to maintain the shield integrity define the maximum numerical aperture (NA) of the optical system. The first mirror aperture can be of the order of 100 mm, which define NA ≈ 0.19. The optimum resolution (R), without aberration of the optical system, is also determined by NA, by means of the well-known formula: $R = \frac{\lambda}{2NA}$, with λ the wavelength at which the object is imaged. So taking into account the requirements of 1 mm resolution or less, at $\lambda = 550\,\mathrm{nm}$, NA $> 3 \cdot 10^{-4}$. For the power transmission (T), NA also plays a role. In our case, the first mirror of the system is the defining aperture, so the best expected power transmission, without accounting for the reflectance of the mirrors, is simply given by the solid angle under which the first mirror sees the object. For a cir-

ISBN 978-3-95450-141-0

cular aperture, T = 1 − cos(arcsin(NA)). So the larger NA, the larger the transmission. With NA ≈ 0.19, T ≈ $1.6 \cdot 10^{-4}$. Finally, one must account for the Depth of Field (DoF), due to the source plane non orthogonal to the main optical axis. Similar to the R, DoF is associated to NA: DoF = λ/NA^2. As is well-known, a larger DoF imposes a lesser resolution (i.e. a larger R). Optical system performance for the imaging system are summarised in Table 1.

Table 1: Summary of the Optical System Properties as Given by the ZEMAX Primary Design and Compared to the Expected Conceptual Approach

	Expected Values		ZEMAX Design
Mag.	0.05 - 0.2		0.085
NA_{eff}	R < 1 mm DoF > 1 mm T > 0.01	> 0.0003 < 0.022 > 0.14	0.01
DoF (mm)	> 4		5
R (μm)	< 1000		30
Δ_{PSF} (mm)	< 1		2-4
Geo. T			$5 \cdot 10^{-5}$

ZEMAX Design

The design of the optical system is mainly done using ZEMAX [3]. The system is divided in three parts, a primary imaging system, which constitute a 3-mirror system block. Their function is to make a first intermediate image of the PBW. Then a series of also 3-mirror block relay imaging systems, to carry the image to the radiation safe area. The last system block performs the image on the camera. This way, by splitting the system in small blocks, we may control aberration and field distortion. With the three mirrors assembly, we should be able to satisfy Petzval condition for each block assembly, and eventually for the whole system assembly. However, in our preliminary design, shown in Fig. 1, we have introduced afocal system block assembly to save distance and keep a small number of mirrors. By doing this, we also introduced coma aberration, and field distortion, which reflects in the Δ_{PSF} value shown in the Table 1. This will have to be corrected in the next design iteration.

Proton Current Density Source

There are several sources to take into account for the imaging of the proton current density distribution: the Optical Transition Radiation (OTR) occurring at the interface between the PBW and the He-filled atmosphere of the Target monolith; the luminescence from specific coating of the PBW; the proton induced fluorescence from the He gas. The OTR is likely to be excluded: the OTR yield from Al to air per 2 GeV proton per unit steradian over the whole visible range is of the order of 10^{-7}. A macro-pulse would generate ≈ 10^8 photons over 2 π steradian. The transmission of the optical system associated with NA, Table 1, excludes the possibility to get any sensible information by means of OTR. The yield from luminescence is much brighter than OTR; there are several possible coating to be used. For example, the typical yield for a Cr:Al2O3 coating is of the order of 10^2 photons per steradian [4]. It is thus expected to get 10^{11} photons per macro-pulse on the sensor. With this level of photon intensity a large signal to noise ratio is expected with the possibility to not only perform single shot image of the macro-pulse, but also it may permits faster acquisition at 10^4 images per second. Finally, the proton induced fluorescence of He-gas may lead to similar photon yield. However, this source is longitudinally extended and provides an additional challenge to the imaging system, which would have either to have infinite depth of field or be telecentric. Both would impose a rather small NA, perhaps incompatible with the resolution requirements.

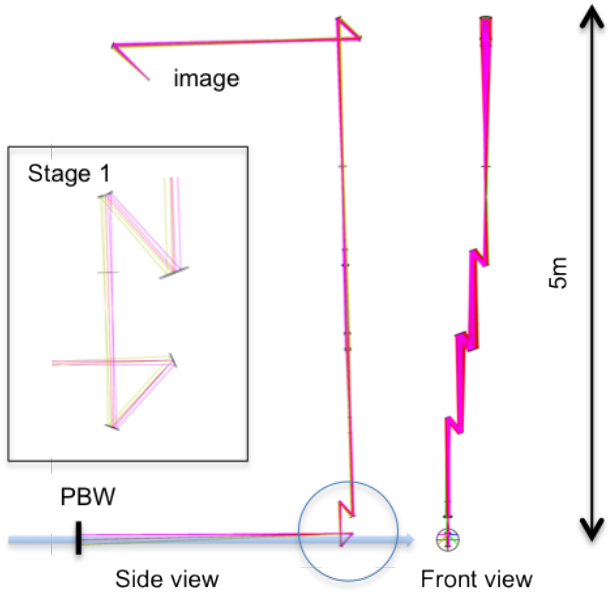

Figure 1: Optical imaging system preliminary design. The proton beam is shown by the semi-transparent arrow; the primary imaging assembly in the inset. The distance between PBW and first mirror is 2.65 m. On the top, the visible beam exits the monolith through a viewport (not shown) and then is finally focused on the image sensor.

IMAGE FAILURE MODE DETECTION

The typical image to be seen from one macro-pulse been swept in horizontal and vertical axes, with a saw-tooth signal of frequency 40 and 29 kHz in Hor. and Vert. respectively, is shown in Figure 2. To generate this image we build a model of the rastering beamlet throught the window. The 4 raster magnets induce a sawtooth motion on both horizontal and vertical axes of the center of mass of the beamlet. With no rastering, the r.m.s beam size is expected to be 12 × 4 mm. So we can generate the image of the current density by summing 2D-Gaussian distributions with their centre of mass

ISBN 978-3-95450-141-0

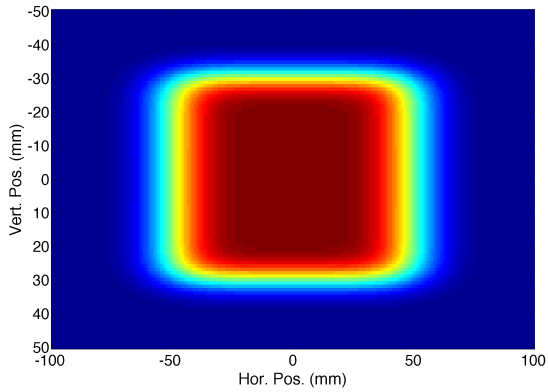

Figure 2: Image of the current density under normal operation.

moved using the parametric equations generated by the raster motion:

$$C_i = B_{0,i} + 2\frac{B_i}{\pi}\arcsin\left(\sin\left(2\frac{\pi}{p_i}t\right)\right) \quad (1)$$

with C_i the centre of mass in the plane i (Hor. or Vert.), $B_{0,i}$ the initial offset of the beam at the time $t = 0$, B_i the amplitude of the motion given by the strength of the magnets, p_i the period of the motion in the plane i, and t the time during which the motion occurs.

In addition, the intensity of the beamlet Gaussian distribution is also time dependent.

This model allows to investigate almost all possible failing modes. For instance, off-centered beam in one or both axis, deflection amplitude not matching the required one, in one or both axis; sweeping may stop at any time through the motion, etc.

In order to be able to detect any of the possible faults, we build the following detection model: the image of the beam with the required condition is generated, and can be compared with the running condition, e.g. beamlet size, beam motion amplitude. Then during commissioning and operation, this generated reference image may be used and compared with each and every image of the macro-pulses. The comparison to be made is given by:

$$r = \sqrt{\sum_{i,j}\frac{\left(\frac{A_{ij}^{PBW}}{A_{ij}^{ref}} - 1\right)^2}{n_x n_y}} \quad (2)$$

with A_{ij}^{PBW}, A_{ij}^{ref} the matrix elements of the real macro-pulse image and the reference image respectively; $n_{x,y}$ the number of lines and columns of the images. r is then a number between 0 and 1.

Some of the possible failure mode are illustrated in Fig. 3. We have assumed a mismatch of the amplitude of the centroid motion induced by the 4 raster magnets. The curves represent the cases in which the horizontal, the vertical, and then both axis amplitudes are smaller than the set values. The

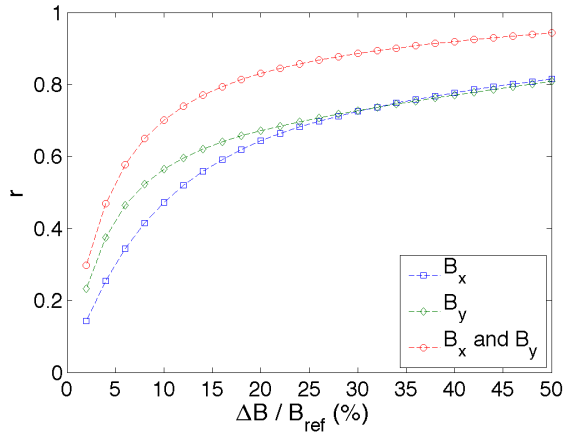

Figure 3: Image residual as given by Eq. 2 for several test failures involving magnet power supply been smaller than the targeted values. The horizontal axis shows the relative difference of the motion amplitude to the nominal one.

calculation of r from Eq. 2 shows for all considered cases, deviation of 5% of the amplitudes of the raster magnets intensities leads to a residual larger than $r \geq 0.2$. Obviously, further investigation of the model is required. We show here that wrong motion amplitude can be detected. However, robustness of the model needs to be demonstrated. In such a case, we will conclude the model and the test to be applicable for the protection of the PBW and the target.

HARDWARE AND FPGA FOR MPS

As discussed above, images of the proton beam current density distribution must be acquired and processed within a single shot period to permit the protection of the PBW. For that, the real-time response of the data acquisition board must be evaluated. In this section, we discuss how the image data is taken to the FPGA digitizer board in the µTCA.4 crate, that equip a Xilinx component, and then elaborated in order to have a response fast enough to satisfy the Machine Protection System (MPS) requirements.

Firstly, the camera interface protocol needs to be selected within existing standardization committees and standards, e.g. Camera Link and Camera Link HS, GigE Vision, USB3 Vision, EMVA 1288, Fire Wire, CoaXPress, and others; at this point in time, the choice of the protocol yet has to be done. It depends strongly on the sensor/camera choice. Intimate to this choice is the selection of a specific board: it can be either FPGA Mezzanine Card (FMC), or Rear Transition Modules (RTM), depending on the selected platform. In addition, once the board is chosen, the connection technology is defined. For instance, the relative decoding/encoding intellectual property is designed to extract the image data from the protocol frame, and to interface the controls for the specific camera. Further integration has to take into account the image data format delivered by a specific camera (RGB24/32, IUV, etc..) and pixel order. This operation of conversion and pixel re-ordering can also be implemented in the FPGA

ISBN 978-3-95450-141-0

processing board, before making any further elaboration. At this point the raw image data, after this pre-elaboration, is stored in memory and can be collected from EPICS for archiving purpose. The next FPGA board operation is frame processing. Two possible scenario are anticipated. The first one is to acquire a single shot image during the passage of a single macro-pulse. This corresponds to the acquisition and processing of the images discussed in the previous section. The second one, is to acquire a series of images shot during the passage of a macro-pulse. This can be done with a fast camera that can be triggered and operated in burst mode. The typical camera speed in view for this acquisition mode is of the order of $20 \cdot 10^3$ frames per second. In this mode, the processing of the images will give information on the beamlet within a macropulse. This is not discussed here. In both acquisition modes, the FPGA board has to be triggered and synchronised with the ESS timing system (essentially a Timing Receiver board). It is required for the FPGA board to control the camera, and to select the images to be acquired and processed.

The image processing to be implemented into the FPGA board will be the following: firstly, the images acquire will have to be normalised to the maximum image intensity. Then the image will be compared to the generated reference image in order to produce the test scalar r (Eq. 2). Finally r will be compared to a threshold producing a boolean value for the MPS trigger.

Normalisation of the acquired images can be implemented following several possible sequences of operation: one of these is to find the largest pixel intensity, then scale the reference image, prior to the division and subtraction operations. However, the exact final sequence of operations will be defined by the time cost of the total operation to produce r. For example, to perform the division it is possible to use the LogiCORE IP Divider Generator, in High Radix implementations that uses the XtreamDSP slices; using the dual-port block RAM, it is possible to write the data in the memory, coming from the pre-elaboration, at the protocol rate, while it is possible to read out, to perform the residual calculation, at an higher rate to reduce the latency of the algorithm. The division in Eq. 2 could be done again using the LogiCORE IP Divider Generator, but could be also a simple factor 2 scaling, in case that the window dimension ($n_x n_y$) is a power of 2. The accumulation is performed using a XtreamDSP slices, and the calculation of the square root is performed using the Xilinx LogiCORE IP CORDIC. A schematic of the FPGA architecture is shown in Fig. 4. It illustrates the essential functionality to be provided by the FPGA board. It includes the acquisition operation of the images, and their processing to extract the boolean value for the MPS trigger. The processing of the fast acquisition frames during one macro-pulse is not treated here. however, the FPGA architecture would be essentially the same, to permit MPS trigger within one macro-pulse.

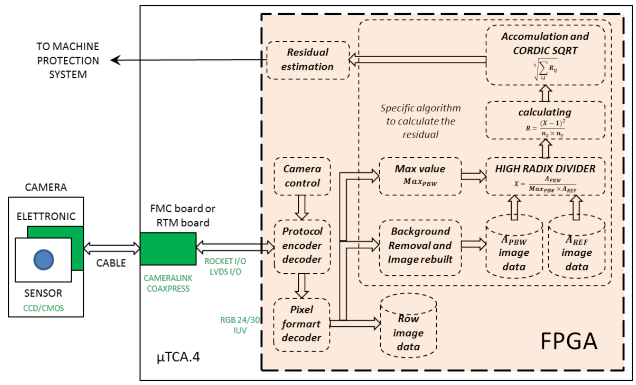

Figure 4: FPGA Architecture.

CONCLUDING REMARKS

For the monitoring and protection of the PBW and TW, we are designing a complex optical system which satisfies image performance together with Target shield requirements. As in any optical system, NA drives the imaging performance. With the requirements drawn, we expect NA ≈ 0.01 to satisfy DoF and resolution requirements. However, This is done to the detriment of the geometrical transmission, and thus imposes a high source radiation yield. This might be satisfied by specific luminescent coating. For instance, Cr:Al2O3 coating may generate enough photons for imaging, but it has a decay time comparable to the macro-pulse duration. This might be an issue and it needs to be addressed. We have developed a model of the expected proton beam density distribution during the rastering operation. This model can be used to investigate all possible failure modes. The model, once validated will be implemented in the FPGA for the image processing and for MPS trigger. Finally, we designed the core architecture for the camera control and FPGA code to be developed, identifying all elements and functionality required for PBW and TW window monitoring and protection.

REFERENCES

[1] M. Eshraqi, H. Danared, D. McGinnis, "Design Options of the ESS LINAC", Proceedings of IPAC2013, THPWO072, pages 3921–3923, Shangai, 2013.

[2] T.J. Shea, C. Bohme, B. Cheymol, S. Gallimore, H. Hassanzadegan, E.J. Pitcher, H. Thomsen, "Proton Beam Measurement Strategy for the 5 MW European Spallation Source Target", Proceedings of IBIC2013, TUPC02, pages 349–352, 2013.

[3] www.zemax.com

[4] T.J. Shea, C. Maxey, T.J. Mcmanamy, D. Feldman, R. Fiorito, A. Shkvarunets, "Status of Beam Imaging Developments for the SNS Target", Proceedings of DIPAC2009, MOOC04, pages 38–40, 2009.

ISBN 978-3-95450-141-0